Acta of Bioengineering and Biomechanics
Vol. 13, No. 4, 2011

Original paper

Microscale analysis of strain–stress state for TiN nanocoating of POLVAD and POLVAD_EXT

ANDRZEJ MILENIN, MAGDALENA KOPERNIK*

AGH University of Science and Technology, Kraków, Poland.

The main purpose of the research was to develop the micromodel of biocompatible titanium nitride nanocoating deposited on polymer by pulsed laser deposition method in blood chambers of Polish ventricular assist devices: POLVAD and POLVAD_EXT. The analysis of the parameters of micromodel crucial for the phenomenon of loss of cohesion occurring between coating and substrate was carried out as well. The micromodel takes into account residual stress, material model of nanocoating, stress resulting from blood pressure in chamber, the thickness of coating and wave parameters of nanocoating (wavelength and antinode). The investigation shows that thickness and residual stress are the most influential parameters. The phenomenon of the loss of cohesion will be observed more frequently for thicker coatings with higher residual stresses.

Key words: *polymer, finite element method (FEM), representative volume element (RVE), titanium nitride (TiN), ventricular assist device (VAD), nanocoating*

1. Introduction

The implantation of blood chamber of Polish ventricular assist device (POLVAD) has become a vital necessity and based on the current state of knowledge anyone is convinced of this fact. Using biocompatible TiN nanocoating [3] on the surface of POLVAD [14] is quite controversial, mainly due to the possibility that the connection between TiN nanocoating and polymer loses cohesion and that other negative phenomena can occur (thrombus formation). These phenomena have very negative consequences for a patient, especially under the cyclic working conditions of blood chamber of VAD.

Thus, the VAD design used by the authors of the present paper is unique because of the deposited TiN nanocoating by using PLD (pulsed laser deposition) method, which is not reported by other researchers. The multiscale model for the analysis of the strain and stress states of multilayer wall of blood chambers of POLVAD and POLVAD_EXT (the second version of POLVAD) was developed and tested in our previous works [10], [12]. However, the model was simplified and many key parameters in microscale were not included. The micromodel was applied in the macromodel of POLVADs, where the maximum values of strain and stress were observed – between two connectors (the most probable failure-source regions). The detailed numerical comparison of two versions of macromodels of POLVADs can be found in [11].

The first goal of the present work is achieved by the development of a new version of the micromodel. The second goal of the present paper is focused on the analysis of the selected parameters of the micromodel. In the micromodel, the following parameters of the phenomenon of loss of cohesion between nanocoating and substrate are investigated:

- The geometry of nanocoatings: antinode and the wavelength of nanocoating as well as the thickness of nanocoating.

* Corresponding author: Magdalena Kopernik, AGH University of Science and Technology, al. Mickiewicza 30, 30–059 Kraków, Poland. Tel.: +48 (12) 617 38 66, fax: +48 (12) 617 29 21, e-mail: kopernik@agh.edu.pl

Received: July 18th, 2011
Accepted for publication: November 14th, 2011

• The mechanical properties of nanocoating – residual stress.

The simulations in microscale are performed for mulitlayer materials of POLVAD and POLVAD_EXT under loading and off–loading conditions.

2. Theory – microscale model

The methods of solving the problems arising from the reproduction of the irregular shape of surface of nanocoatings in micromodels are presented below. The approach, which describes in a simplified way the problems associated with the surface defects, was shown in [1]. The roughness of nanocoating was approximated by surface wave defined using antinode and wavelength [16] in some approaches to the analysis of the phenomenon of loss of cohesion for nanocoatings represented by titanium nitride deposited on substrate by PVD (physical vapour deposition) process. A very interesting approach to the description of the roughness of nanocoating is the use of fractal (Cantor set [2] and the theory of Koch [6]) and artificial neural networks [5] for generating the roughness of coatings. These solutions are observed particularly in modelling the wear of the tools covered with hard nanocoatings such as TiN.

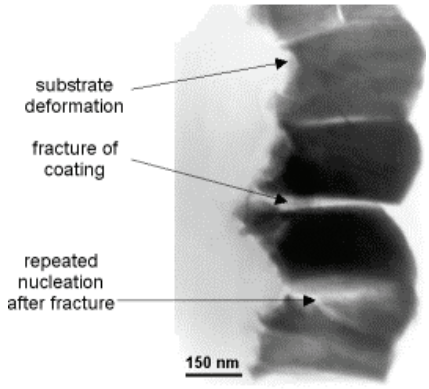

Fig. 1. FEM microstructure of 350 nm TiN coating deposited on polymer by PLD method

The new finite element micromodel of POLVADs (POLVAD and POLVAD_EXT) was developed using experimental data [8] presented in figure 1 and was further used for the analysis of its selected parameters, but the values of the parameters were differentiated according to factor analysis [9]. In the present work, the improvements in the microscale model are based on introducing the irregularities (roughness) of the surface of TiN nanocoating represented by periodic function with key parameters of the wave of surface (antinode, wavelength), the thickness of nanocoating and residual stress, because in microscale the roughness of nanocoating surface influences stress and strain states.

The developed micromodel of POLVADs is based on a representative volume element (RVE) composed of substrate (polymer) material layer and very thin TiN nanocoating deposited on it. For the construction of micromodel, the data from the macromodel of POLVADs (boundary conditions) are necessary, therefore, the parameters corresponding to the macroscale, i.e., macroparameters, will be marked with a superscript *M*, for example, macrostress σ^M. On the contrary, the parameters corresponding to the RVE in microscale (microparameters) will be marked with a superscript *m*, for example, microstress σ^m. All average values of the symbols referring to the RVE will be marked with an upper bar, for example, mean microstress $\overline{\sigma}^m$. The macrostress σ_{ij}^M and macrostrain ε_{ij}^M tensors corresponding to a certain point X^M in the macromodel can be evaluated directly by the average volume of microstress σ_{ij}^m and microstrain ε_{ij}^m over RVE.

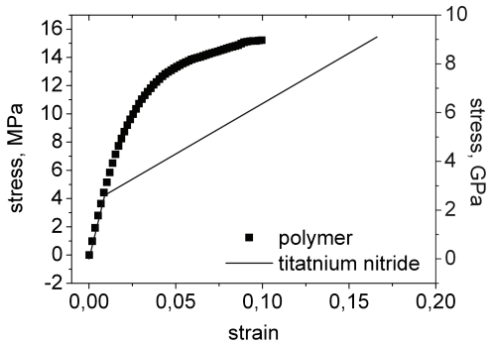

Fig. 2. The material models of TiN and polyurethane

A the $2\frac{1}{2}$ D FEM micromodel of POLVADs has 4-node finite elements used to solve the boundary problem [7]. The material model of TiN was identified in the previous work [8] using inverse analysis. The parameters of bilinear material model of TiN were identified by the authors and are shown in figure 2, as well as the results of the tension test performed for polymer [4]. Thus, it is clearly underlined that the nonlinearity of mechanical properties between TiN coating and polymer really exists. The assumption of the elastic–plastic and nonlinear elastic material models is justified. Considering such phenomena as elastic, elastic–plastic deformation and unloading process (in the elastic–plastic case) allows the boundary

problem in the microscale to be solved by the FEM micromodel. The initial stress $\{\sigma^m_{0\text{res}}\}$ in TiN nanocoating is taken into account in the FEM formulation. The relation between stresses and strains is represented by the matrix (vector) definition:

$$\{\sigma^m\} = [D^m]\{\varepsilon^m\} - \{\sigma^m_{0\text{res}}\}, \tag{1}$$

where:

$\{\sigma^m_{0\text{res}}\}$ – residual stresses;

$\{\sigma^m\}$ and $\{\varepsilon^m\}$ – stress and strain tensors, respectively, in vector format [7].

The variational principle of the nonlinear elastic and elastic–plastic theory leads to the following functional form for finite element *e* in the RVE:

$$W = \int_{V_e} \frac{1}{2}\{U^m\}^T[B]^T[D^m][B]\{U^m\}dV - \int_{V_e}\{U^m\}^T[B]^T\{\overline{\sigma}^m_{0\text{res}}\}dV - \int_{S_e}\{U^m\}^T[\overline{N}]^T\{p^m\}dS, \tag{2}$$

where:

$\{U^m\}$ – displacement vector in nodes of elements;

$\overline{\sigma}^m_{0\text{res}}$ – experimental value of initial stress in current finite element *e*.

The values of $\overline{\sigma}^m_{0\text{res}}$ in nanocoatings for different thicknesses of TiN are based on the results described in [8].

The effective Young's modulus is used instead of the Young's modulus in the elastic zone in order to linearize the functional (equation (2)) for nonlinear problem:

$$E^m_p = \frac{\sigma^m_i}{\varepsilon^m_i}. \tag{3}$$

The stiffness matrix $[K]$ and load vector $\{F\}$ are as follows:

$$[K^m_e] = \int_{V_e}[B]^T[D^m][B]dV, \tag{4}$$

$$\{F^m_e\} = \int_{V_e}\{U^m\}^T[B]^T\{\overline{\sigma}^m_{0\text{res}}\}dV - \int_{S}[\overline{N}]^T\{p^m\}dS. \tag{5}$$

A comparison between literature studies and the results reached for biocompatible TiN nanocoating deposited on polymer by using PLD method shown in [8] leads to conclusion that the values of compressive residual stresses are higher for TiN nanocoating deposited by PLD method. These stresses are observed in many studies of this type of materials and can be attributed to the influence of surface tension and may be due to the influence of the conditions for the layer formation. Summarizing, the initial stresses (residual stresses) in TiN nanocoating result from deposition process and must be evaluated before the simulation of loading. In the present work, the experimental residual stress is interpreted as a mean stress and is localized in a thin TiN coating. The simulations of loading and unloading stages in the microscale are possible after implementing $\overline{\sigma}^m_{0\text{res}}$. The residual stress applied in the micromodels in comparison with the stresses reached in the macromodel of POLVADs after active loading is very high [10], [11]. High values of residual stresses play a crucial role in the modelling because of the cyclic loading applied in VADs, which can cause the propagation of the loss of cohesion in the boundaries between hard TiN nanocoating and soft substrate (polymer).

The representative volume element is an intermediate scale between the micro- and macroscales. The following types of boundary conditions on surface of RVE can be imposed:

- Kinematic boundary conditions:

$$U^m_i = \varepsilon^M_{ij} x_i. \tag{6}$$

- Static boundary conditions:

$$n_i\sigma^m_{ij} = n_i\sigma^M_{ij}. \tag{7}$$

The average stress inside the RVE is equal to σ^M_{ij}.

- Periodic boundary conditions: displacement component perpendicular to the side of the RVE is imposed, but the ones parallel to the side are let free. In this case, each side of RVE is a symmetric plane.

A problem solved by applying different types of boundary conditions will not predict the same behaviour for the RVE [17]. In the case considered, all types of boundary conditions do not provide any information necessary for the microscale analysis. Generally, Periodic Boundary Conditions (PBCs) are usually preferred, because they provide the most reasonable estimation of mechanical properties of heterogeneous materials, even if the structure of RVE is not periodic [15]. In our case, the PBCs are used in the direction parallel to the surface of blood chamber, and the static BCs are applied in the direction of blood pressure. Considering the TiN nanocoatings of POLVADs, the following modification of PBCs is proposed. The deformation tensor is taken from the macroscale in modelling the boundary conditions of the RVE. The direction of normal to the surface of RVE for TiN nanocoating corresponds to the direction of hydro-

static pressure p (blood pressure p^m). Therefore, shear stresses and strains are not present on this surface and stress p is one of the principal stresses of the stress tensor. Thus, the solution in main coordinate system is found. The principal strains can be used as boundary conditions. Each side of the RVE is a symmetry plane with these boundary conditions, because the shear stresses and strains equal zero. A 2½ boundary problem is considered. The strain ε_2^M (the second principal strain of strain tensor) is introduced into the microscale as a constant. Therefore, a 3D boundary problem of the RVE deformation is transformed into a 2D plane strain problem with the current value of ε_2^M. The principal strain ε_1^M and pressure $p^M = p^m = p$ are also used in the model of the RVE. Concluding, the boundary conditions are changed from microscale to macroscale in this stage of modelling.

3. Results and discussion

The numerical experiment was based on factor analysis [9]. The 132 simulations were run for micromodels built for two versions of blood chamber of POLVADs (POLVAD and POLVAD_EXT) under loading (16 kPa) and off-loading conditions. The results were scanned from critical points of micromodel (the wave nodes of the surface of nanocoating). All the results obtained are shown in tables 1–6 and in figures 3–8 (units are the same in tables and in figures). The thickness of the specimen of micromodel analyzed in the simulations is H_{RVE} = 1850 nm and the width is W_{RV} = 6000 nm. The following symbols of micromodel were used in tables 1–6 and in their captions:

- H_{TiN} – the thickness of nanocoating,
- A – the antinode of the surface of nanocoating,
- L – the wavelength of the surface of nanocoating,
- $\sigma_{0\,\mathrm{res\,TiN}}$ – a residual stress of nanocoating,
- $\sigma^m_{0\,\max}$ – a maximum mean stress of micromodel,
- $\sigma^m_{xy\,\max}$ – a maximum plane stress of micromodel,
- $\varepsilon^m_{i\,\max}$ – a maximum effective strain of micromodel.

The results of modelling the TiN nanocoating under off-loading conditions are presented in tables 1–2 for two wavelengths. The observations made on the basis of these results reveal that for the same residual stresses introduced the computed strains are greater in the thicker coatings than in the thinner ones. The compressive mean stresses obtained are higher in thinner coatings. The mean stresses are lower in thicker coatings, but the values of their parameters are similar to the values of tension stresses. Thus, for thicker coatings the phenomenon of the loss of cohesion will be observed more frequently. The differences in the models are very slight between the computed strains and comparable between the coatings of different wavelengths. The differences in the coatings of different wavelengths are visible for the values of stresses. The lower mean stresses are calculated for coatings of smaller wavelengths; however, plane stresses are higher for these coatings.

Table 1. Modelling TiN nanocoating under off-loading conditions for A = 50 nm and L = 350 nm

	H_{TiN}	$\sigma_{0\,\mathrm{resTiN}}$	$\sigma^m_{0\max}$	$\sigma^m_{xy\max}$	$\varepsilon^m_{i\max}$
	nm	GPa	GPa	GPa	
1	50	–2.0	–1.125	0.17	0.0037
2	350	–2.0	–0.760	0.27	0.0053
3	350	–0.5	–0.220	0.067	0.0013
4	50	–0.5	–0.285	0.050	0.00087

Table 2. Modelling TiN nanocoating under off-loading conditions for A = 50 nm and L = 150 nm

	H_{TiN}	$\sigma_{0\,\mathrm{resTiN}}$	$\sigma^m_{0\max}$	$\sigma^m_{xy\max}$	$\varepsilon^m_{i\max}$
	nm	GPa	GPa	GPa	
1	50	–2.0	–1.108	0.23	0.0035
2	350	–2.0	–0.716	0.22	0.0047
3	350	–0.5	–0.193	0.058	0.0012
4	50	–0.5	–0.277	0.058	0.0008

The examples of local distributions of computed mean stress, plane stress and effective strain for micromodels are shown in figures 3–4 for cases 1 and 2 from table 1. These results were reached for the same wavelengths and residual stresses, but for different thicknesses of the deposited coatings. The distributions of the selected parameters show that for thicker coatings the gradients of the computed parameters are smaller. The gradients of the calculated parameters are bigger in the thinner coatings. The character of the distributions of selected parameters is similar for thin and thick coatings for the same wavelengths and residual stresses. The effect of the thickness of coating on the character of distribution was examined.

The next examples of the local distributions of the computed mean stress, plane stress and effective strain for micromodels are shown in figure 5 for case 2 presented in table 2. Figures 4 and 5 present the coatings of the same thicknesses and residual stresses, but

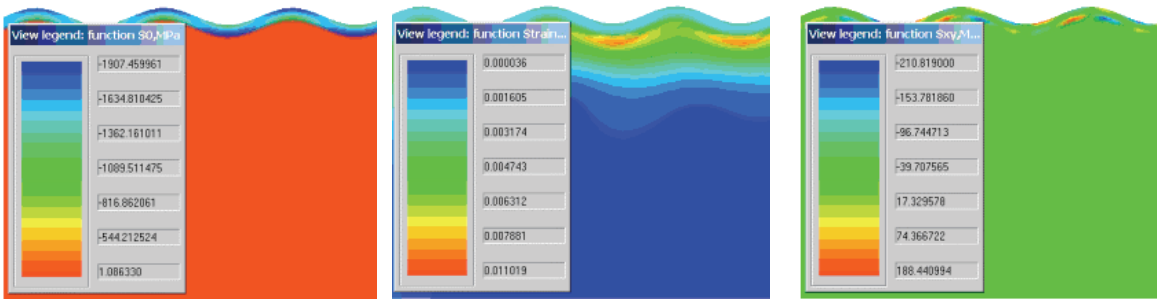

a b c

Fig. 3. The local micromodel results for case 1 from table 1: a) mean stress, b) effective strain and c) plane stress

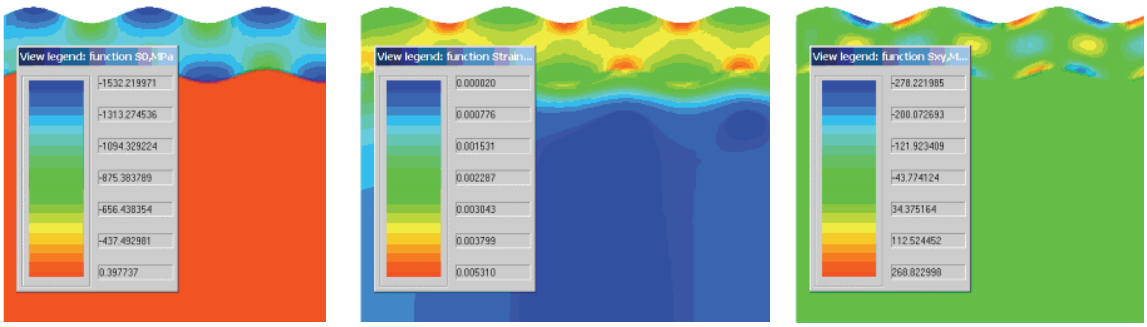

a b c

Fig. 4. The local micromodel results for case 2 from table 1: a) mean stress, b) effective strain and c) plane stress

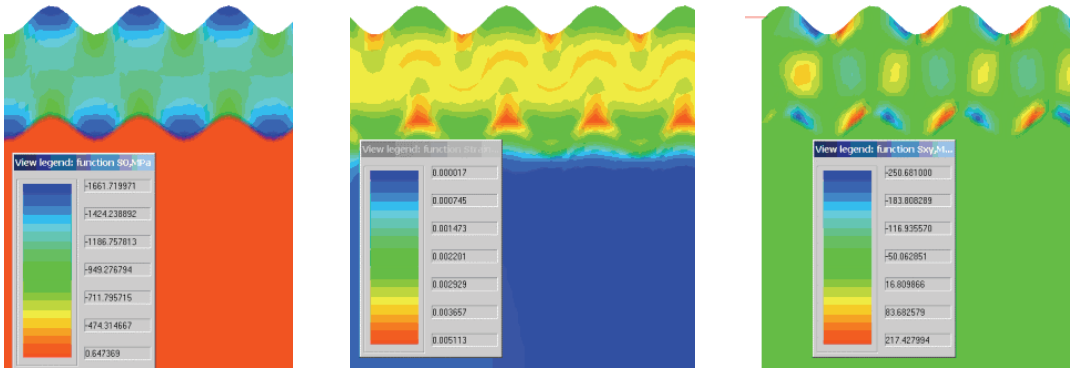

a b c

Fig. 5. The local micromodel results for case 2 from table 2: a) mean stress, b) effective strain and c) plane stress

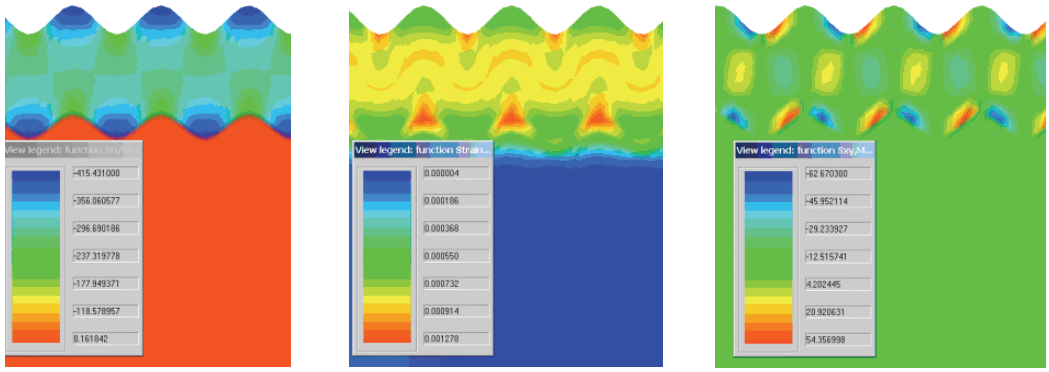

a b c

Fig. 6. The local micromodel results for case 3 from table 2: a) mean stress, b) effective strain and c) plane stress

different wavelengths. In figure 5, coatings have smaller periods in comparison with coatings shown in figure 4 and, therefore, all the computed parameters have smaller values in figure 5. The distributions of the calculated parameters have similar character, but denser surface of coatings (smaller wavelengths) is responsible for the lower values of the computed parameters ("spring effect"). The influence of the wavelength of coating on the character of distribution was investigated.

The local distributions of the computed mean stress, plane stress and effective strain for micromodels are depicted in figure 6 for case 3 from table 2. In figures 5 and 6, there are shown the coatings of the same thicknesses and wavelengths, but of different residual stresses. In figure 6, coatings have lower residual stresses in comparison with coatings shown in figure 5 and, consequently, in figure 6 all the values of the computed parameters are several times smaller. The distributions of the calculated parameters have similar character, but due to higher residual stresses the values of the calculated parameters are higher. The influence of the residual stress of coating on the character of distribution was analyzed.

The results represented by the distributions of the selected parameters shown in figures 5 and 6 reproduce exactly a real situation presented in figure 1. The wavelengths and thickness of coatings in figures 5 and 6 are similar to these in the specimen in figure 1. This specimen was not deformed under working loadings, but prepared for TEM (transmission electron microscopy) analysis using microtome technique. The distributions of effective strains and plane stresses testify to the occurrence of fracture. The distributions of effective strains and plane stresses show such gradients of computed parameters that can cause cracking similar to the result visible in figure 1. The maximum values of effective strains for two different residual stresses are:

- 0.0047 for 2 GPa,
- 0.0012 for 0.5 GPa.

These values of parameters are lower than the values characteristic of elastic region of very thin titanium nitride (compare, figure 2 and [8]). It should be noted that the value of effective strain (0.009) for elastic region of titanium nitride is achieved for very thin TiN coating (50 nm) and not for 350 nm (figure 1). Summarizing, the comparison between micromodel and real specimen leads to the conclusion that for thicker coatings the cracking is observed at lower values of effective strain than for thin coatings.

Table 3. Modelling TiN nanocoating under loading conditions for A = 50 nm and L = 350 nm (POLVAD)

	H_{TiN}	$\sigma_{0\,\mathrm{resTiN}}$	$\sigma^m_{0\max}$	$\sigma^m_{xy\max}$	$\varepsilon^m_{i\max}$
	nm	GPa	GPa	GPa	
1	50	–2.0	–1.113	0.26	0.0039
2	350	–2.0	–0.601	0.32	0.0058
3	350	–0.5	–0.093	0.093	0.0017
4	50	–0.5	–0.233	0.075	0.0011
5	200	–2.0	–0.624	0.393	0.0056
6	350	–1.0	–0.312	0.169	0.003
7	200	–0.5	–0.1	0.114	0.002
8	50	–1.0	–0.61	0.138	0.0017
9	200	–1.0	–0.216	0.209	0.004

Table 4. Modelling TiN nanocoating under loading conditions for A = 50 nm and L = 150 nm (POLVAD)

	H_{TiN}	$\sigma_{0\,\mathrm{resTiN}}$	$\sigma^m_{0\max}$	$\sigma^m_{xy\max}$	$\varepsilon^m_{i\max}$
	nm	GPa	GPa	GPa	
1	50	–2.0	–1.057	0.245	0.0037
2	350	–2.0	–0.642	0.247	0.0049
3	350	–0.5	–0.105	0.072	0.0014
4	50	–0.5	–0.228	0.071	0.001
5	200	–2.0	–0.543	0.281	0.006
6	350	–1.0	–0.29	0.131	0.003
7	200	–0.5	–0.073	0.082	0.0016
8	50	–1.0	–0.638	0.129	0.0015
9	200	–1.0	–0.237	0.148	0.0025

Table 5. Modelling TiN nanocoating under loading conditions for A = 50 nm and L = 350 nm (POLVAD_EXT)

	H_{TiN}	$\sigma_{0\,\mathrm{resTiN}}$	$\sigma^m_{0\max}$	$\sigma^m_{xy\max}$	$\varepsilon^m_{i\max}$
	nm	GPa	GPa	GPa	
1	50	–2.0	–1.127	0.250	0.0037
2	350	–2.0	–0.762	0.309	0.0048
3	350	–0.5	–0.154	0.082	0.0013
4	50	–0.5	–0.350	0.066	0.00068
5	200	–2.0	–0.635	0.271	0.0052
6	350	–1.0	–0.355	0.121	0.0024
7	200	–0.5	–0.183	0.071	0.0012
8	50	–1.0	–0.714	0.121	0.0013
9	200	–1.0	–0.366	0.138	0.0024

Table 6. Modelling TiN nanocoating under loading conditions for A = 50 nm and L = 150 nm (POLVAD_EXT)

	H_{TiN}	$\sigma_{0\,\mathrm{resTiN}}$	$\sigma^m_{0\max}$	$\sigma^m_{xy\max}$	$\varepsilon^m_{i\max}$
	nm	GPa	GPa	GPa	
1	50	–2.0	–1.3	0.237	0.0027
2	350	–2.0	–0.849	0.239	0.0047
3	350	–0.5	–0.165	0.064	0.0012
4	50	–0.5	–0.357	0.063	0.0007
5	200	–2.0	–0.756	0.271	0.005
6	350	–1.0	–0.344	0.122	0.002
7	200	–0.5	–0.190	0.075	0.0012
8	50	–1.0	–0.655	0.121	0.0013
9	200	–1.0	–0.288	0.138	0.003

The results for the micromodels of the wall of POLVADs (POLVAD and POLVAD_EXT) loaded with blood pressure for two wavelengths of surface are presented in tables 3–6, but earlier the computed strain and stress states were reached by applying the blood pressure (loading) in the macromodels prepared for both versions of blood chambers. Afterwards the micromodel is used exactly in these regions, where in the macromodel of POLVADs the maximum values of strain and stress are observed – between two connectors (the most probable failure-source regions) [10], [11]. The following maximum values of the strains observed in the failure-source regions are introduced into the micromodel:

- POLVAD: $\varepsilon_1 = 0.0002$; $\varepsilon_2 = 0.0002$; $p = 16$ kPa.
- POLVAD_EXT: $\varepsilon_1 = 0.0001$; $\varepsilon_2 = -0.00005$; $p = 16$ kPa.

The analysis of the results presented in tables 3–6 obtained from the micromodels loaded with blood pressure for materials of POLVAD and POLVAD_EXT shows that the highest mean compressive stresses are concentrated in POLVAD_EXT. The plane stresses are lower for POLVAD_EXT than for POLVAD. The effective strains reached in the micromodels prove to be higher in POLVAD than in POLVAD_EXT. The calculated effective strains occur in elastic zones of materials in both versions of VADs.

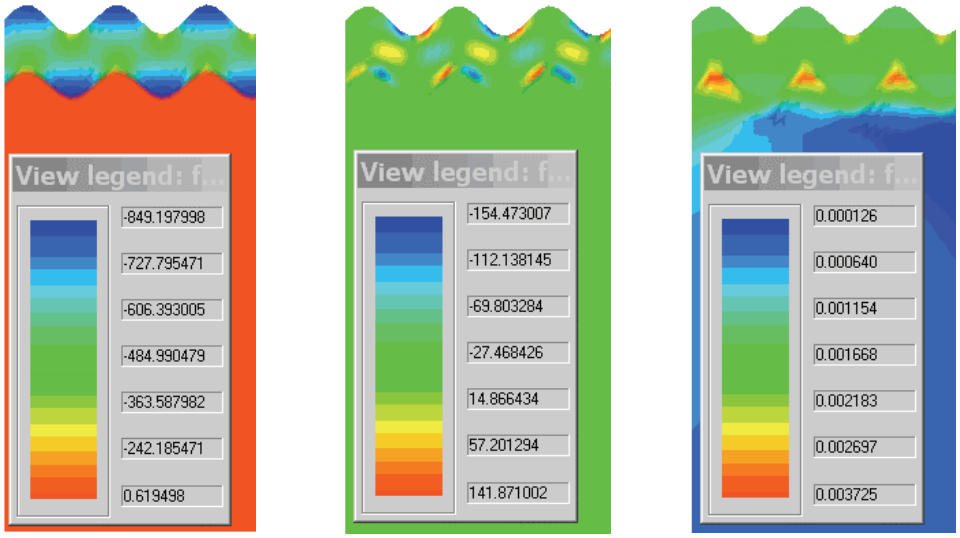

a b c

Fig. 7. The local micromodel results for case 9 from table 4: a) mean stress, b) effective strain and c) plane stress

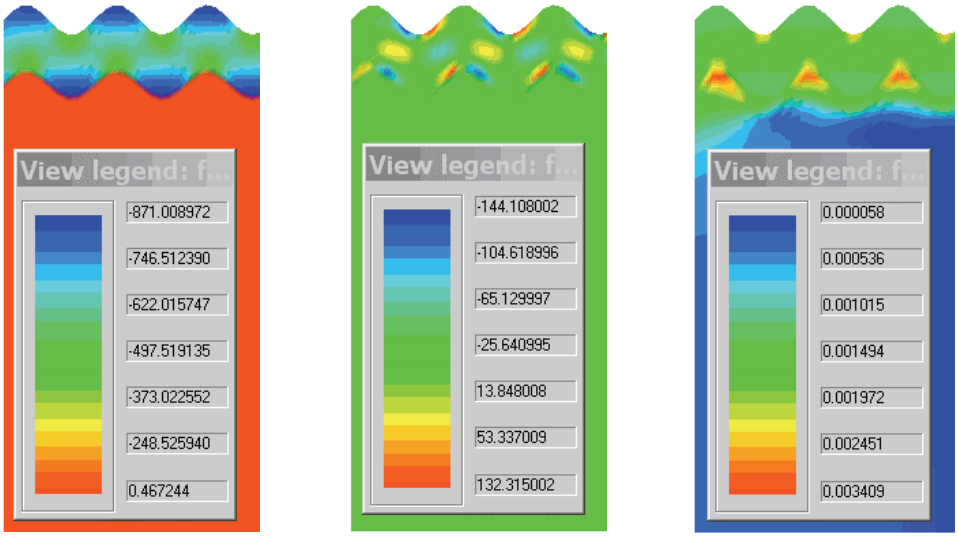

a b c

Fig. 8. The local micromodel results for case 9 from table 6: a) mean stress, b) effective strain and c) plane stress

The characters of the distributions of the computed parameters are the same for loaded (figures 7 and 8) and off-loaded micromodels (figures 3–6). Therefore, the influence of the thickness, wavelength and residual stress of coatings on the character of distributions for loaded and off-loaded micromodels is similar under these two loading conditions. The difference in the characters of distributions between the micromodels of two versions of POLVADs is shown in figures 7 and 8. In the micromodels analyzed, the thickness (200 nm) and residual stress (1 GPa) are the middle values of all examined values of the selected parameters. Both micromodels presented in figures 7 and 8 have the same wavelength equal to 150 nm, because at lower values of the period the "effect of spring" is more clearly visible – lower values of the computed parameters are induced. There is no difference in the character of the local distribution of selected parameters between POLVAD and POLVAD_EXT, the differences are observed only for the values of the computed parameters which are discussed in the analysis of results presented in tables 3–6.

4. Csonclusions

- The new version of the micromodel of the wall of POLVADs developed in authors' FEM computer program is helpful in reaching the goals established:

Simulating in microscale the stress and strain states for the failure-source regions distinguished in the macromodel of the wall of POLVADs.

Analyzing the parameters crucial for the phenomenon of the loss of cohesion.

- The results reached after the loading of blood pressure show that the biggest gradients of stresses are observed in the nanocoating and on the boundaries of TiN/polymer in micromodel which can lead to fracture. The lower plane stresses and effective strains are reached in the micromodel of POLVAD_EXT. The highest values of mean compressive stresses are observed for the POLVAD micromodel.

- The analysis of the values of parameters crucial for the phenomenon of the loss of cohesion under conditions without blood loading shows that the most influential parameters of the micromodel of TiN/polymer are thickness and residual stress. On the contrary, wavelength is less influential parameter with respect to the strains reached in simulation. The wavelength of the wave of the surface of TiN is more influential with respect to the computed stresses.

- The analysis of the local distributions of parameters crucial for the phenomenon of the loss of cohesion for the micromodel of TiN/polymer reveals smaller gradients for thicker coatings. The denser surface of coatings (smaller wavelengths) is responsible for the lower values of parameters ("spring effect"). The phenomenon of the loss of cohesion will be observed more frequently for thicker coatings, because their values of compressive mean stresses are similar to the values of tension stresses. There is no difference in the character of the local distribution of selected parameters between POLVAD and POLVAD_EXT, the differences are only observed in the values of the calculated parameters.

- The comparison between the micromodel of TiN/polymer and a real specimen leads to the conclusion that for thicker coatings the cracking is observed at lower values of effective strain than for thin coatings.

Acknowledgements

Financial assistance of the MNiSzW, project No. 2011/01/D/ST8/04087, is acknowledged.

References

[1] BENARDOS P.G., VOSNIAKOS G.-C., *Predicting surface roughness in machining: a review*, International Journal of Machine Tools and Manufacture, 2003, 43, 833–844.

[2] CHEN Y., FU P., ZHANG Ch., SHI M., *Numerical simulation of laminar heat transfer in microchannels with rough surfaces characterized by fractal Cantor structures*, International Journal of Heat and Fluid Flow, 2010, 31, 622–629.

[3] EBNER R., LACKNER J.M., WALDHAUSER W., MAJOR R., CZARNOWSKA E., KUSTOSZ R., LACKI P., MAJOR B., *Biocompatibile TiN-based novel nanocrystalline films*, Bulletin of the Polish Academy of Sciences, Technical Sciences, 2006, 54, 167–173.

[4] EL FRAY M., *Elastomerowe biomateriały polimerowe o polepszonej odporności zmęczeniowej dla potrzeb protez serca*, Biuletyn Programu Polskie Sztuczne Serce, 2011, 5, 18–23.

[5] GRZESIK W., BROL S., *Hybrid approach to surface roughness evaluation in multistage machining processes*, Journal of Materials Processing Technology, 2003, 134, 265–272.

[6] KANG M.Ch., KIM J.S., KIM K.H., *Fractal dimension analysis of machined surface depending on coated tool wear*, Surface and Coatings Technology, 2005, 193, 259–265.

[7] KOPERNIK M., MILENIN A., *The sensitivity analysis of nanoindentation test for specimen composed of TiAlN and TiN using the mathematical model*, Steel Research International, 2008, 79, 555–562.

[8] KOPERNIK M., MILENIN A., MAJOR R., LACKNER J.M., *Identification of material model of TiN using numerical simulation of nanoindentation test*, Materials Science and Technology, 2011, 27, 604–616.

[9] KRZANOWSKI W.J., *Principles of multivariate analysis*, Oxford University Press, New York, 2000.

[10] MILENIN A., KOPERNIK M., *The multiscale FEM model of artificial heart chamber composed of nanocoatings*, Acta of Bioengineering and Biomechanics, 2009, 11, 13–20.

[11] MILENIN A., KOPERNIK M., *Comparative analysis of ventricle assist devices POLVAD and POLVAD_EXT based on multiscale FEM model*, Acta of Bioengineering and Biomechanics, 13, 2011, 13–23.

[12] MILENIN A., KOPERNIK M., *FEM code for the multi-scale simulation of the stress–strain state of the blood chamber composed of polyurethane and TiN nanocoating*, Computer Methods in Materials Science, 2011, 11, 215–222.

[13] NALBANT M., GÖKKAYA H., TOKTAS I., SUR G., *The experimental investigation of the effects of uncoated, PVD- and CVD-coated cemented carbide inserts and cutting parameters on surface roughness in CNC turning and its prediction using artificial neural networks*, Robotics and Computer-Integrated Manufacturing, 2009, 25, 211–223.

[14] SARNA J., KUSTOSZ R., MAJOR R., LACKNER J.M., MAJOR B., *Polish Artificial Heart – new coatings, technology, diagnostics*, Bull. Pol. Ac. Tech., 2010, 58, 329–335.

[15] THIBAUX P., CHASTEL Y., CHAZE A.M., *Finite element simulation of a two-phase viscoplastic material: calculation of the mechanical behaviour*, Comput. Mater. Sci., 2000, 18, 118–125.

[16] WIKLUND U., GUNNARS J., HOGMARK S., *Influence of residual stresses on fracture and delamination of thin hard coatings*, Wear, 1999, 232, 262–269.

[17] ZIENKIEWICZ O.C., TAYLOR R.L., *The finite element method*, Butterworth–Heinemann, London, 2000.